A Land Surface Process/Radiobrightness Model with Coupled Heat and Moisture Transport in Soil

Yuei-An Liou, *Member, IEEE,* and Anthony W. England, *Fellow, IEEE*

***Abstract*—Heat and moisture transport in soil are coupled processes that jointly determine temperature and moisture profiles. We present a physically based, one-dimensional (1-D), coupled heat and moisture transport hydrology (1-DH) model for bare, unfrozen, moist soils subject to insolation, radiant heating and cooling, and sensible and latent heat exchanges with the atmosphere. A 60-day simulation is conducted to study the effect of dry-down on soil temperature and moisture distributions in summer for bare soil in the Midwest United States. Given a typical initial moisture content of 38% by volume, we find that temperature differences between the water transport and no water transport cases exhibit a diurnal oscillation with a slowly increasing amplitude, but never exceed 4.4 K for the 60-day period. However, moisture content of the surface decreases significantly with time for the water transport case and becomes only about 21% at the end of the same period.**

The 1-DH model is linked to a radiobrightness (1-DH/R) model as a potential means for soil moisture inversion. The model shows that radiobrightness thermal inertia (RTI) correlates with soil moisture if the two radiobrightnesses are taken from times near the thermal extremes, e.g., 2 a.m. and 2 p.m., and that RTI appears temperature-dependent at the ending stages of the dry-down simulations where soils are dry and their moisture contents vary slowly. Near times of thermal crossover, the RTI technique is insensitive to soil moisture.

I. Introduction

THE NEAR-SURFACE distributions of moisture and temperature influence the exchanges of moisture and energy between land and atmosphere, and, through these processes, affect weather and climate [1]–[7]. Atmospheric models that are used to study or predict weather or climate rely upon embedded land surface process (LSP) models to estimate moisture and energy transfer within soils and vegetation that result in the land-atmosphere exchanges. LSP models, like the biosphere-atmosphere transfer scheme (BATS) [8] or the simple biosphere model (SiB) [9], characterize these transfer processes with relatively simple, almost cartoon-like parameterizations of the actual biophysical processes. The relative simplicity of these LSP models permits computational efficiencies in the demanding environment of numerical modeling of weather or climate.

Most LSP models are tuned to reproduce observed temperatures, humidities, and winds in the boundary layer rather than reproduce good estimates of moisture and temperature in the underlying soil or vegetation. It is possible to replace the LSP model with a one-dimensional hydrology (1-DH) model of the surface processes to achieve a greater fidelity in moisture and temperature profiles. While such use of a 1-DH model is currently too computationally intensive for most atmospheric modeling applications, the approach can be used retrospectively to yield running estimates of water stored in soil at specific points [10]–[12] or over selected regions. Because a 1-DH model will accumulate errors over time in its estimate of stored water, the approach is potentially more powerful if point estimates can be checked periodically against an actual measurement or if regional estimates can be refined through the assimilation of remotely sensed data. This process might also be used to examine the possible equivalence between an LSP model's estimate of soil wetness and the 1–DH/radiobrightness (1-DH/R) model's estimate of stored water.

Of available remotely sensed data, radiobrightnesses are arguably the single class of measurements that are most sensitive to the critical parameters of surface temperature and moisture [13]–[17]. While L-band radiobrightness is recognized as the most desirable of the possibilities [16], radiobrightness at any frequency where emissivity is influenced by the Debye relaxation of water will be sensitive to moisture in vegetation or at the surface of bare soil. We have modeled and observed this sensitivity in field experiments at 19.35 and 37.0 GHz [18]. As satellite radiometers achieve adequate spatial resolutions at frequencies below the Special Sensor Microwave/Imager's (SSM/I's) 19 GHz, their sensitivities to soil moisture will become increasingly pronounced. For the purposes of this investigation, we focus on the temporal signature of radiobrightness at the SSM/I frequencies of 19.35, 37.0, and 85.5 GHz because these data have been available on a near-daily basis for the all of the Earth since 1987 [19].

Several investigators have developed one-dimensional (1-D) thermal/emission models to predict thermal infrared (TIR) or thermal microwave (radiobrightness) signatures over a diurnal cycle for discrimination among rock types in TIR images [20] and among various soils [21], for inference about soil moisture [22]–[25], and for mapping frozen and thawed prairie soils [26]. The diurnal thermal/radiobrightness model of England [25] was expanded to simulate annual thermal and radiobrightness for dry soil [27]. Results from the annual model demonstrate that the seasonal history significantly influences the surface temperature. Liou and England [28] recently

Manuscript received February 9, 1996; revised April 25, 1997. This work was supported by NASA Grant NAGW-3430.

Y.-A. Liou is with the Center for Space and Remote Sensing Research, National Central University, Chung-Li, Taiwan, R.O.C. (e-mail: yueian@csrsr.ncu.edu.tw).

A. W. England is with the Department of Electrical Engineering and Computer Science and the Department of Atmospheric, Oceanic and Space Sciences, The University of Michigan, Ann Arbor, MI 48109-2122 USA (e-mail: england@eecs.umich.edu).

Publisher Item Identifier S 0196-2892(98)00223-X.

improved this annual thermal model to include freezing and thawing of soil moisture. However, none of these thermal models accounts for vertical transport of water in soil which is a dominant process governing temperature and moisture profiles and, consequently, TIR and radiobrightness signatures.

In this paper, we develop a 1-dimensional hydrology/radiobrightness (1-DH/R) model for unfrozen soils that incorporate coupled thermal and water transport. Radiobrightness is based upon a quasispecular, microwave emission model [24], [27], and [28], which should be appropriate for 19.35 GHz over bare or sparsely vegetated soil, but increasingly less appropriate at 37.0 and 85.5 GHz where most soil surfaces appear increasingly rough.

Philip and de Vries [29] and de Vries [30] proposed a coupled heat and moisture transfer model for porous materials. In their work, liquid and vapor flux densities accounted for the total moisture flux density and liquid water was continuously in equilibrium with water vapor. Heat conduction, transfer of latent heat by vapor movement, and transfer of sensible heat in vapor and liquid comprised the total heat flux in a porous, unsaturated soil. Heat transfer by convection and radiation within the soil was assumed to be negligible. Moisture and temperature distributions in the soil were obtained by solving two coupled, nonlinear, partial differential equations in time and space.

Many attempts have been made to refine or support the Philip and de Vries theory. Working with laboratory soil columns, Gee [31] found that the theory predicted a moisture flux which was one half to one third that observed in a silt loam at intermediate water content. In a fine sandy loam soil at low soil water content, Cassel *et al.* [32] showed that the predicted net flux agreed with observation. Jackson *et al.* [33] evaluated the theory for a clay loam soil under field conditions and found it adequate at intermediate soil water content, but an isothermal theory was better at high and very low water contents. Kimball *et al.* [34] applied the coupled theory to calculate soil heat fluxes in a field of Avondale loam. They obtained a fair agreement with observation only after modifying the air shape factor curve and ignoring heat transfer due to water vapor movement. They concluded that situation-specific "calibrations" are required to reliably use the coupled theory.

Milly and Eagleson [35], [36] and Milly [37], [38] developed a matric-head formulation for simultaneous moisture and heat flow based upon the water-content formulation of Philip and de Vries. One of their goals was to generalize the Philip and de Vries' theory to accommodate the complications of hysteresis and inhomogeneity. Bach [39] used the Milly and Eagleson formulation to study thermally driven water movement in Otero sandy loam soil and concluded that the Philip and de Vries theory provided an adequate description of nonisothermal transport processes. Other examples concerning coupled heat and moisture transport that are based upon the Philip and de Vries theory include Abdel-Hadi and Mitchell [40], Shah *et al.* [41], Thomas [42], Ewen and Thomas [43], and Thomas and King [44].

The Philip and de Vries theory will be adopted in this study because its strengths and weaknesses are relatively well understood by the soil science community, and it appears to be the best theory available. Improved models for thermal conductivity [45], vapor diffusion coefficients [34], tortuosity factor for diffusion of gases in soil [46], and water retention [47] are incorporated in the original theory. For the purposes of this paper, we ignore hysteresis because our interest is in simulations of soil dry-down and not of infiltration.

The governing equations for the heat and moisture transport are too complicated to be solved analytically. Camillo *et al.* [48] used a finite difference, numerical scheme with variable depth step. In their method, heat and moisture fluxes at all depths and at the surface were first computed. From these fluxes, they found the change in heat and moisture contents, and, hence, temperature and moisture content per unit volume for all layers. The process was repeated until the solutions met their criterion for convergence that the absolute value of the change in surface temperature between iterations was less than 0.1 K for all times in a diurnal cycle. Their solutions were compromised because no convergence criterion was required for moisture transport at the land-air boundary. We improve upon the Camillo *et al.* model by using the Newton–Raphson method to match both heat and moisture fluxes at the land-air interface. To reduce the possibility of errors in the 1-DH model caused by omission of historical land-air exchanges of energy, initial temperatures and a continuing thermal flux at the lower boundary that is appropriate for time-of-year are obtained from the annual thermal model by Liou and England [28].

Based upon simulations using the 1-DH/R model, we discuss the effects of vertical transport of moisture in soil upon soil temperature, moisture profiles, and upon radiobrightness signatures for a 60-day simulation of drying in summer. Also, we reexamine the feasibility of the radiobrightness thermal inertia (RTI) measure of soil moisture [25].

II. Land Surface Process Model

Our 1-DH model concerns vertical heat and moisture transfer in unsaturated soil, and at the land-air interface. For the soil, we chose a silt loam, a typical soil type in the Midwest U.S., which consists of 19% sand, 22.5% clay, and 58.5% silt, and has a porosity of 48% [28]. The thermal and hydraulic properties of the soil-water system can be inferred from the soil texture and moisture content. These properties are thermal conductivity, heat capacity, liquid and vapor diffusivity, hydraulic conductivity, and water retention. Thermal conductivity and heat capacity have been presented in [28]; the other parameters are reviewed here.

A. Governing Equations of Heat and Moisture Transfer

The equations governing heat and moisture transport in soil may be derived from the equations for heat and moisture (liquid water, ice, and vapor) conservation, i.e.,

$$\frac{\partial X_m}{\partial t} = -\nabla \cdot \vec{q}_m \tag{1}$$

$$\frac{\partial X_h}{\partial t} = -\nabla \cdot \vec{q}_h \tag{2}$$

where

X_m total moisture content per unit volume, kg/m^3;

X_h total heat content per unit volume, J/m^3;

t time, s;

$\vec{q}_m = \vec{q}_v + \vec{q}_l$ vector moisture flux density, kg/m^2-s, where $\vec{q}_v$ and $\vec{q}_l$ are the vector vapor and liquid flux densities, respectively;

$\vec{q}_h$ vector heat flux density, J/m^2-s.

For unfrozen ground, moisture and heat content per unit volume are

$$X_m = \rho_l\theta_l + \rho_v\theta_a \tag{3}$$

$$X_h = (C_d + c_l\rho_l\theta_l + c_p\rho_v\theta_a)(T - T_0) + L_{v_0}\rho_v\theta_a - \rho_l\int_0^{\theta_l} W\,d\theta \tag{4}$$

respectively, where

ρ_l density of the liquid water, kg/m^3;

θ_l volumetric liquid water content, m^3/m^3;

ρ_v density of water vapor, kg/m^3;

θ_a volumetric air content, m^3/m^3;

C_d volumetric heat capacity of dry porous medium, J/m^3-K;

c_l specific heat of liquid water at constant pressure, J/kg-K;

c_p specific heat of water vapor at constant pressure, J/kg-K;

T temperature, K;

T_0 reference temperature, K;

L_{v_0} latent heat of vaporization at reference temperature, J/kg;

W is the differential heat of wetting [30], J/kg.

Following Philip and de Vries [29] and de Vries [30], the heat and moisture flux densities are described by

$$\frac{\vec{q}_m}{\rho_l} = -D_T\nabla T - D_\theta\nabla\theta_l - K\hat{k} \tag{5}$$

$$\vec{q}_h = -\lambda\nabla T + L_{v_0}\vec{q}_v + c_p(T - T_0)\vec{q}_v + c_l(T - T_0)\vec{q}_l \tag{6}$$

respectively, where

$D_T = D_{T_l} + D_{T_v}$ thermal moisture diffusivity, m^2/K-s;

$D_\theta = D_{\theta_l} + D_{\theta_v}$ isothermal moisture diffusivity, m^2/s;

D_{T_l} thermal liquid diffusivity;

D_{T_v} thermal vapor diffusivity;

D_{θ_l} isothermal liquid diffusivity;

D_{θ_v} isothermal vapor diffusivity;

K hydraulic conductivity, m/s;

$\hat{k}$ vertical unit vector;

λ thermal conductivity of a moist, porous medium, J/m-K-s.

Upon substituting (3)–(6) into (1) and (2), we get two coupled, nonlinear, partial differential equations for heat and moisture transfer, i.e.,

$$\begin{aligned}&\left[1 + \frac{(S-\theta_l)\rho_0}{\rho_l}\frac{\partial h_r}{\partial\theta_l} - \frac{\rho_v}{\rho_l}\right]\frac{\partial\theta_l}{\partial t} + \frac{(S-\theta_l)}{\rho_l}\left(h_r\frac{\partial\rho_0}{\partial T} + \rho_0\frac{\partial h_r}{\partial T}\right)\frac{\partial T}{\partial t}\\ &= \nabla\cdot(D_T\nabla T + D_\theta\nabla\theta_l + K\hat{k})\end{aligned} \tag{7}$$

$$\begin{aligned}&\left[L_v(S-\theta_l)\rho_0\frac{\partial h_r}{\partial\theta_l} - L_v\rho_v - \rho_l W\right]\frac{\partial\theta_l}{\partial t}\\ &+ \left[C + L_v(S-\theta_l)\left(h_r\frac{\partial\rho_0}{\partial T} + \rho_0\frac{\partial h_r}{\partial T}\right)\right]\frac{\partial T}{\partial t}\\ &= \nabla\cdot[(\lambda + L_v\rho_l D_{T_v})\nabla T] + L_v\rho_l\nabla\cdot(D_{\theta_l}\nabla\theta_l)\\ &+ \rho_l[(c_pD_{\theta_v} + c_lD_{\theta_l})\nabla\theta_l\\ &+ (c_pD_{T_v} + c_lD_{T_l})\nabla T + c_pK\hat{k}]\cdot\nabla T.\end{aligned} \tag{8}$$

We have used

$$\rho_v = \rho_0 h_r \tag{9}$$

$$\theta_a = S - \theta_l \tag{10}$$

$$L_v = L_{v_0} + (c_l + c_p)(T - T_0) \tag{11}$$

in (7) and (8) where

ρ_0 density of saturated water vapor, kg/m^3;

h_r relative humidity;

S porosity.

Equations (7) and (8) are highly nonlinear in moisture and temperature because both thermal and hydraulic properties of the soil-water system are functions of moisture and temperature. They can be solved by the following numerical scheme.

B. Finite Difference Scheme

Fig. 1(a) shows the schematic diagram for the division of the soil profile into n layers, where d_i, $i = 1,\ldots,n$, is the thickness of the ith layer, and z_i, $i = 1,\ldots,n$, is the depth from the surface to the center of the ith layer. z_n must be beyond the thermal penetration of the period of interest (approximately less than 1 m for a diurnal case and less than 3 m for a seasonal case). The required number of soil layers is influenced by current and historical weather forcings, the time step of the numerical scheme, and soil texture. We typically use 60 layers in our simulations.

Soil layers near the surface are very likely to be modified by rapidly changing land-air interactions, while those at the bottom of the soil layer are insensitive to transient weather forcing. Consequently, thicknesses of the soil layers must be small near the surface, but may increase with depth. Layer thicknesses of a few tenths of a millimeter or less at the surface are generally required.

Fig. 1(b) is a flowchart of our algorithm for the 1-DH model. Major operations for each time step are listed as follows.

1) Initialize temperature and moisture profiles using results from the annual thermal model [28].
2) Match upper boundary conditions of heat and moisture fluxes using the Newton–Raphson method [49].
3) Compute heat and moisture fluxes between layers (excluding the bottom one) using (7) and (8).
4) Match bottom boundary conditions of heat and moisture fluxes assuming the bottom layer has the same fluxes as the second to bottom layer so that its temperature and moisture content remain constant.
5) Determine the change in temperature and moisture content for all layers.
6) Check if the changes in temperature and moisture content between iterations are less than the criteria for

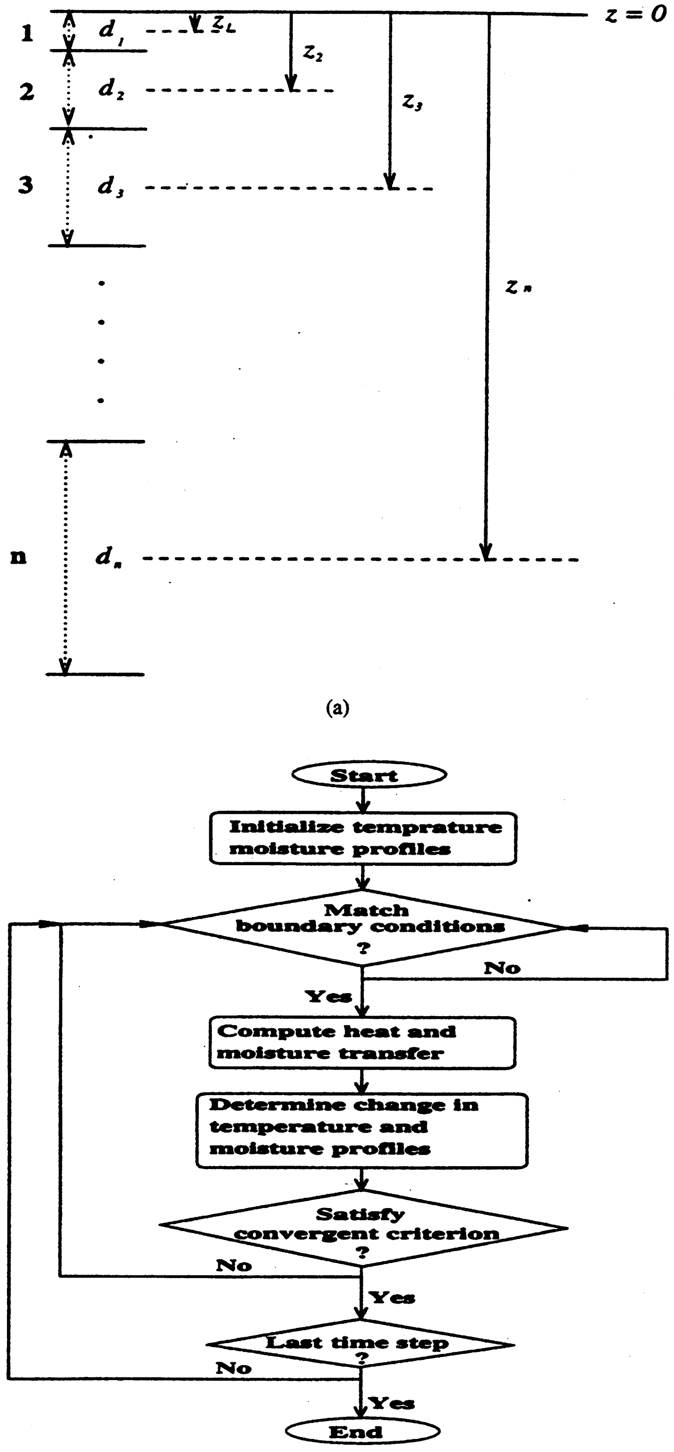

Fig. 1. (a) Schematic diagram for thesoil layers. (b) Flowchart of 1-DH model algorithm.

convergence—0.01 K for temperature and 0.01% for moisture content.

7) If criteria for convergence are not satisfied, then proceed to step 2 and repeat steps 3–5. Otherwise, go to the next time step.
8) If the last time step has not been reached, then go to step 2 and repeat steps 3–6. Otherwise, end the process.

Approximations used in the numerical method were

$$\left(\frac{\partial x}{\partial t}\right)_i \rightarrow \frac{x_{i+1} - x_i}{t_{i+1} - t_i} \tag{12}$$

$$(\nabla x)_i \rightarrow \frac{x_{i+1} - x_i}{z_{i+1} - z_i} \tag{13}$$

$$(\bar{y})_i \rightarrow \frac{y_{i-1} y_i}{y_{i-1} + y_i} \tag{14}$$

where

x_i temperature or moisture content of the ith layer;
y constitutive quantities of those terms within each divergence, such as liquid/vapor diffusivity, latent heat of vaporization, heat capacity, thermal conductivity, liquid/vapor diffusivity, hydraulic conductivity, or their combinations.

C. Boundary Conditions

Boundary conditions include energy and moisture budgets both at the land-air interface and at the bottom of the soil layer. Following Liou and England [28], the energy budget at the land-air interface is a balance among solar radiation, sky brightness, sensible and latent heat transfer, and gray-body emission from the surface. At the bottom of the soil layer, we use a constant energy flux determined from our annual model [28] for the time of year. The moisture budget is assumed to be constant at the bottom of the soil layer. In the absence of precipitation, the moisture budget at the land-air interface is a product of latent heat exchanges between the land and atmosphere.

D. Hydraulic Conductivity and Water Retention

Mualem [50] proposes a closed-form equation for predicting the relative hydraulic conductivity. This model is based upon knowledge of the soil-water retention curve and the hydraulic conductivity at saturation and can be described as

$$K_r = S_e \left[\int_0^{S_e} \frac{1}{\Psi}\, dS_e \bigg/ \int_0^1 \frac{1}{\Psi} S_e \, dS_e \right] \tag{15}$$

$$S_e = \frac{\theta_l - \theta_r}{\theta_s - \theta_r} \tag{16}$$

$$= \left[\frac{1}{1 + (l\Psi)^n}\right]^{1-1/n} \tag{17}$$

where

K_r relative hydraulic conductivity, m/s;
S_e effective saturation;
Ψ matric head, m;
θ_r residual liquid water content, m^3/m^3;
θ_s saturated liquid water content, m^3/m^3;
l, n constants.

Van Genuchten [51] generalizes the Mualem model by expressing the water retention as

$$S_e = \left[\frac{1}{1 + (l\Psi)^n}\right]^m \tag{18}$$

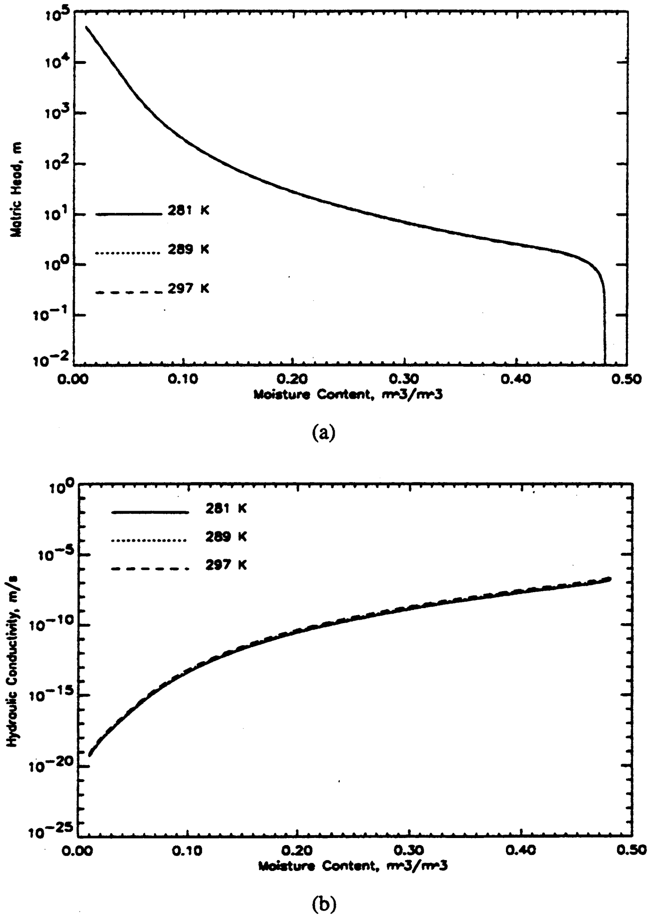

Fig. 2. (a) Soil water retention for the Salkum silt loam. (b) Hydraulic conductivity as a function of moisture content.

where $m = 1-1/n$ for the Mualem model. The van Genuchten model does relatively well for predictions of hydraulic conductivity at high and medium water content, but fails at lower water content [52], [53].

Rossi and Nimmo [47] recently developed two models for soil water retention—the two-parameter sum model and the two-parameter junction model. Both are modified forms of the Brooks and Corey model [54] with residual liquid water content taken as zero and both fit observations over the entire range from saturation to oven dryness for seven sets of soil textural classes. The two-parameter junction model is analytically integrable so that its inclusion in the Mualem hydraulic conductivity model is straightforward. Water retention according to the two-parameter junction model is

$$\frac{\theta_l}{\theta_s} = \theta_1 = 1 - a_1\left(\frac{\Psi}{\Psi_0}\right)^2, \quad 0 \le \Psi \le \Psi_i \tag{19}$$

$$\frac{\theta_l}{\theta_s} = \theta_2 = \left(\frac{\Psi_0}{\Psi}\right)^\eta, \quad \Psi_i \le \Psi \le \Psi_j \tag{20}$$

$$\frac{\theta_l}{\theta_s} = \theta_3 = a_2 \ln\left(\frac{\Psi_d}{\Psi}\right), \quad \Psi_j \le \Psi \le \Psi_d \tag{21}$$

where Ψ_0 and η are the two independent parameters characterizing the system, θ_s and Ψ_d, the value of Ψ at oven dryness, are assigned values based upon the measurements, and a_1, Ψ_i, Ψ_j, and a_2 are parameters that are determined as analytical functions of Ψ_d and η through the following relations:

$$\begin{aligned} \theta_1(\Psi_i) = \theta_2(\Psi_i) \quad & \frac{\partial\theta_1}{\partial\Psi}(\Psi_i) = \frac{\partial\theta_2}{\partial\Psi}(\Psi_i) \\ \theta_2(\Psi_j) = \theta_3(\Psi_j) \quad & \frac{\partial\theta_2}{\partial\Psi}(\Psi_j) = \frac{\partial\theta_3}{\partial\Psi}(\Psi_j). \end{aligned} \tag{22}$$

Thus

$$a_1 = \frac{\eta}{2}\left(1+\frac{\eta}{2}\right)^{-\left(1+\frac{\eta}{2}\right)} \tag{23}$$

$$\Psi_i = \Psi_0\left(1+\frac{\eta}{2}\right)^{1/\eta} \tag{24}$$

$$a_2 = \eta e\left(\frac{\Psi_0}{\Psi_d}\right)^\eta \tag{25}$$

$$\Psi_j = \Psi_d e^{-1/\eta}. \tag{26}$$

Fig. 2(a) shows the water retention curve for the Salkum silt loam, which is found to fit observations very well from saturation to oven dryness [47].

Finally, by applying the two-parameter junction model to the Mualem model, we obtain the relative hydraulic conductivity

$$K_r(\theta_l) = \sqrt{\frac{\theta_l}{\theta_s}}\frac{I^2(\theta_l)}{I^2(\theta_s)} \tag{27}$$

where

$$I(\theta_l) = \begin{cases} I_{\rm III}(\theta_l) & 0 \le \theta_l \le \theta_j \\ I_{\rm II}(\theta_l) & \theta_j \le \theta_l \le \theta_i \\ I_{\rm I}(\theta_l) & \theta_i \le \theta_l \le \theta_s \end{cases}$$

and

$$I_{\rm III}(\theta_l) = \frac{a_2}{\Psi_d}\left[\exp\left(\frac{\theta_l}{a_2\theta_s}\right) - 1\right] \tag{28}$$

$$I_{\rm II}(\theta_l) = I_3(\theta_j) + \frac{\eta}{\Psi_o}(\eta+1) \times \left[\left(\frac{\theta_l}{\theta_s}\right)^{(\eta+1)/\eta} - \left(\frac{\theta_j}{\theta_s}\right)^{(\eta+1)/\eta}\right] \tag{29}$$

$$I_{\rm I}(\theta_l) = I_{\rm II}(\theta_i) + \frac{2a_1^{1/2}}{\Psi_o} \times \left[\left(1-\frac{\theta_i}{\theta_s}\right)^{1/2} - \left(1-\frac{\theta_l}{\theta_s}\right)^{1/2}\right] \tag{30}$$

in which $\theta_i = \theta_l(\Psi_i)$ and $\theta_j = \theta_l(\Psi_j)$ have been used. Subsequently, following Milly [37], one can get hydraulic conductivity

$$K = K(\theta_l, T) = K_0 K_r(\theta_l)\frac{\vartheta(T_0)}{\vartheta(T)} \tag{31}$$

where

K_0 saturated hydraulic conductivity at a reference temperature T_0;

ϑ kinematic viscosity, kg/m-s.

Fig. 2(b) shows the hydraulic conductivity as a function of moisture for the silt loam. Equation (27) is used to estimate the hydraulic conductivity, but its performance has not been validated [47]. Therefore, estimates of the hydraulic conductivity are compared with those computed by Milly [37]. It appears that both models agree on the order of magnitude.

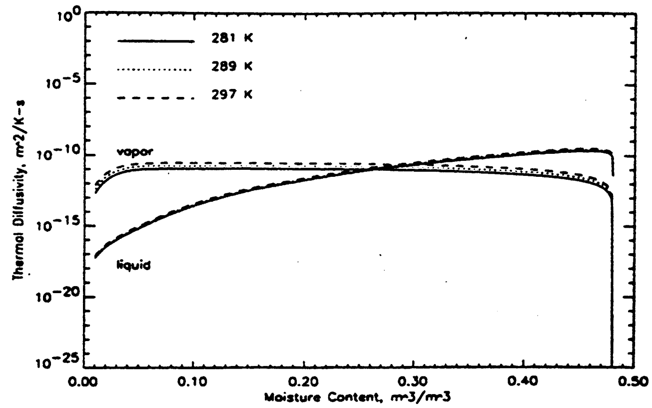

(a)

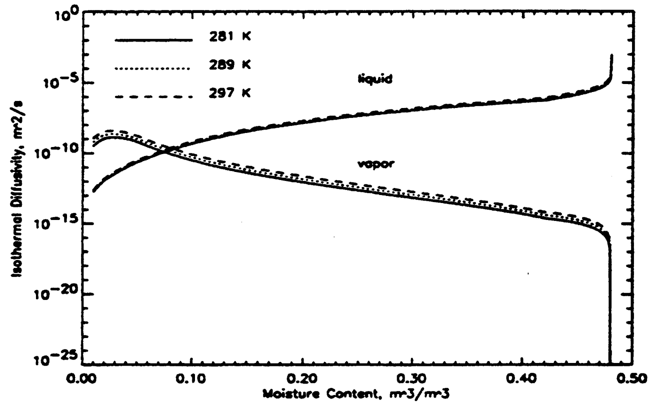

(b)

Fig. 3. (a) Thermal liquid and vapor diffusivities. (b) Isothermal liquid and vapor diffusivities.

E. Liquid and Vapor Diffusivities

From Philip and de Vries [29] and de Vries [30], the moisture- and temperature-dependent liquid and vapor diffusivities can be expressed as

$$D_{T_l} = K\partial\Psi/\partial T \quad (32)$$

$$D_{T_v} = fD_v\nu\beta h_r\zeta/\rho_l \quad (33)$$

$$D_{\theta_l} = K\partial\Psi/\partial\theta_l \quad (34)$$

$$D_{\theta_v} = \alpha\theta_a D_v\nu g\rho_v(\partial\Psi/\partial\theta_l)/\rho_l R_v T \quad (35)$$

where

- $\partial\Psi/\partial T = (\Psi/\sigma)\,d\sigma/dT = \gamma\Psi$, where σ is the surface tension of water, J/m^2, and γ is the temperature coefficient of surface tension of water, K^{-1};
- f = porosity, S, for $\theta_l \leq \theta_{lk}$, $f = \theta_a + \theta_a\theta_l/(S - \theta_{lk})$ for $\theta_l > \theta_{lk}$ is a correction factor for the thermal vapor diffusivity, where θ_{lk} is the value of θ_l at which liquid continuity fails, m^3/m^3;
- $D_v = 4.42 \times 10^{-8}T^{2.3}/P$ is the molecular diffusion coefficient of water vapor in air, m^2/s, where P is the total gas pressure, Pa;
- $\nu = P/(P - p)$ is the mass flow factor, where p is the partial pressure of water vapor, Pa;
- $\alpha = 0.67$ is the tortuosity factor for diffusion of gases in soils;
- $\beta = \frac{d\rho_0}{dT}$, kg/m^3-K, where ρ_0 is the density of saturated water vapor, kg/m^3;
- $\zeta = (\nabla T)_a/\nabla T$, K/m, where ∇T is the average temperature gradient in the porous medium, K/m, and $(\nabla T)_a$ is the average temperature gradient in the air-filled pores, K/m;
- g is the acceleration due to gravity, m/s^2;
- R_v is the gas constant of water vapor, J/kg-K.

Equations (32) to (35) are used to compute the four diffusivities: $D_{T_l}, D_{T_v}, D_{\theta_l}$, and D_{θ_v} with the following modifications:

$$D_v = 0.229(T/273.15)^{1.75} \quad [34], [35] \quad (36)$$

$$\alpha = (S - \theta_l)^{2/3} \quad [46], [38], [55] \quad (37)$$

$$\rho_0 = 10^{-3}e^{19.819-4975.9/T} \quad [34], [55] \quad (38)$$

Liquid and vapor diffusivities are shown in Fig. 3. Since there are no experimental data that can be used to validate the predictions of liquid and vapor diffusivities, computed results are compared with those obtained by Milly [37]. It is found that estimates from the two models agree on the order of magnitude.

F. Simulation

The 1-DH model is run for a 60-day period starting from 06/22 for both water transport and no water transport in soil at a northern latitude of 43.5° (that of Sioux Falls, SD). The initial temperature and moisture profiles of the soil are results from the annual thermal model [28] in which soil moisture was fixed at 38% for all layers.

Fig. 4(a) shows the surface moisture content over the 60-day period for both the water transport and the no water transport cases. For the no water transport case, the surface moisture content is simply constant. For the water transport case, surface moisture content exhibits a small diurnal oscillation with a quickly decreasing average. Diurnal peaks appear during nighttime due to condensation, and valleys appear during daytime due to evaporation. The difference in surface moisture content between the water transport and the no water transport cases approaches 19% at 60 days.

Fig. 4(b) shows constant-moisture curves as a function of depth and day number for the 60-day period for the water transport case. We notice two major characteristics. First, near-surface soils are interacting with the air, while deep soils are not. This is clearly observable since downward-propagating constant-moisture curves exhibit a diurnal oscillation that damps out with depth. Second, there is an expected long-term moisture loss at the surface and a commensurate net upward movement of water, i.e., evaporation dominates over condensation in the latent heat exchange at the land-air interface.

Surface temperatures for the water transport case are shown in Fig. 5(a). Notable characteristics include 1) a strong diurnal oscillation with a slowly increasing average for the first 40 days and a slowly decreasing average after that; and 2) the day-to-night temperature difference increases with day number, from about 16 K at day 1 (06/22) to about 20 K at day 60 (08/20) because the thermal inertia of the soil decreases as the surface soils dry.

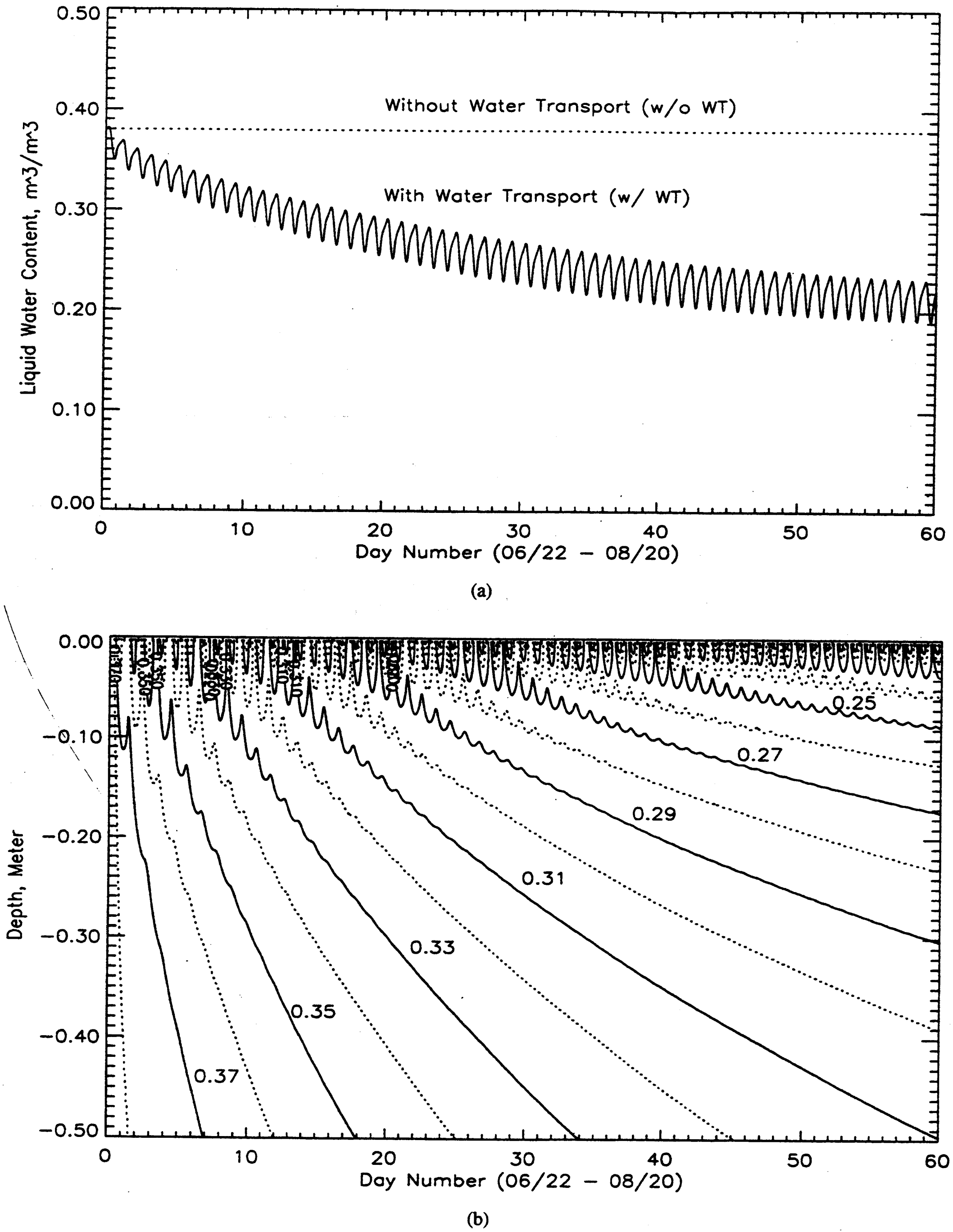

Fig. 4. (a) Soil moisture content at the surface for the water transport and no water transport cases. (b) Soil moisture profile for the water transport case.

The differences in surface temperatures between the water transport and the no water transport cases are shown in Fig. 5(b). They exhibit a small diurnal oscillation with a slowly increasing average and amplitude. The maximum difference is only 4.4 K during daytime at day 60. The difference is small because thermal inertia is the integrated response of the soil over a diurnal cycle which penetrates beyond the dry surface soils.

Fig. 6 shows the soil temperature profile on day 1 for the water transport case. It shows that (1) isotherms are created after sunrise and start to merge some time after peak insolation; (2) temperature gradients in the first few centimeters are much larger during the day than during the night; and (3) diurnal thermal pulses penetrate approximately 50 centimeters. We present only 06/22 isotherms because all diurnal isotherm patterns for the 60-day period were similar.

III. Remote Measure of Soil Moisture

A. Soil Dielectric Properties

Water content and temperature dominate the dielectric properties of soil. Water content is a key parameter because of a significant contrast in permittivity between water and soil constituents. Temperature is important because it governs the

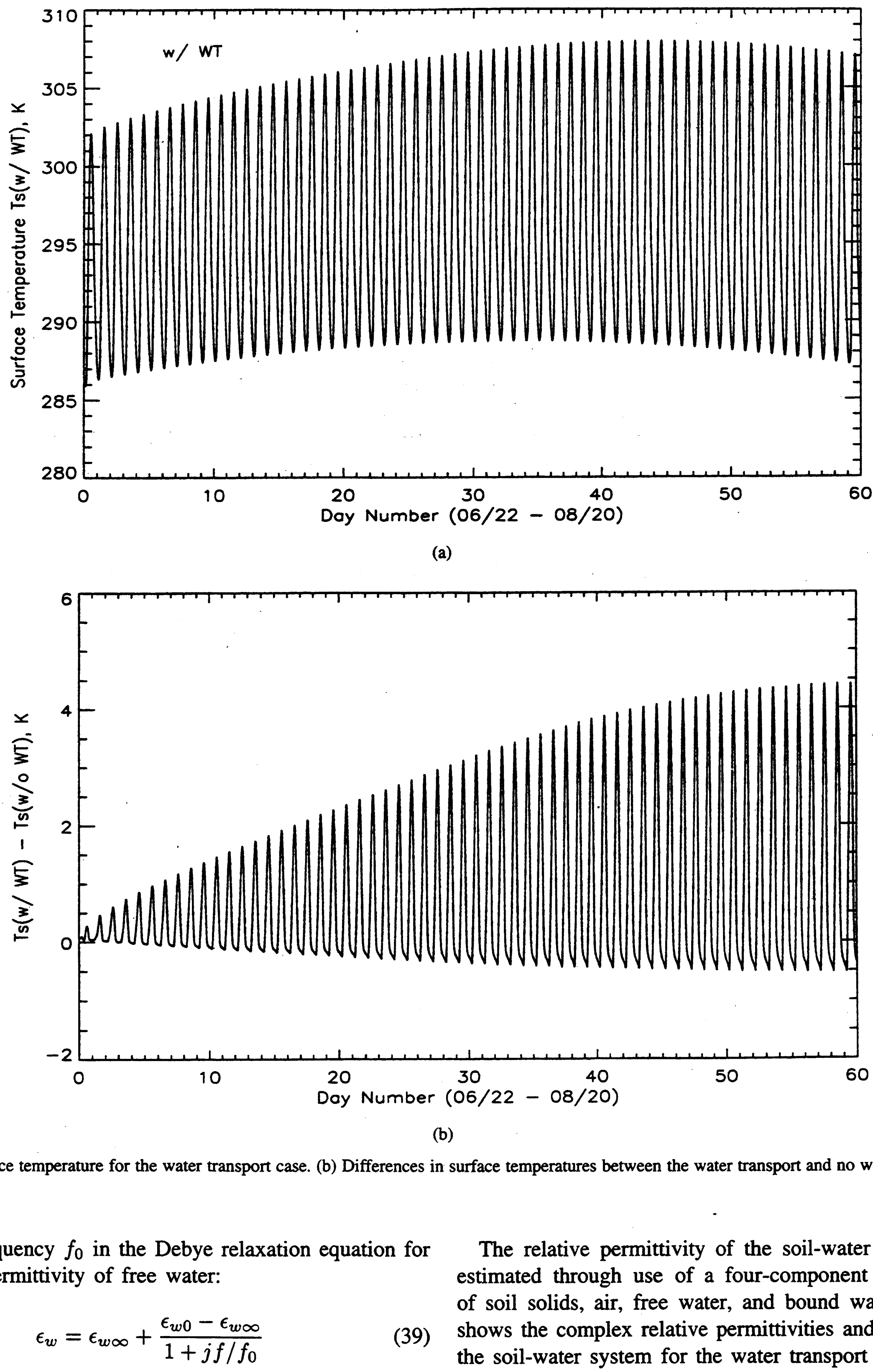

Fig. 5. (a) Surface temperature for the water transport case. (b) Differences in surface temperatures between the water transport and no water transport cases.

relaxation frequency f_0 in the Debye relaxation equation for the relative permittivity of free water:

$$\epsilon_w = \epsilon_{w\infty} + \frac{\epsilon_{w0} - \epsilon_{w\infty}}{1 + jf/f_0} \tag{39}$$

where

ϵ_{w0} static dielectric constant of pure water;
$\epsilon_{w\infty}$ high-frequency limit of ϵ_w;
f frequency, Hz.

For example, the relaxation frequency is about 14.5 GHz at 287 K and 23.5 GHz at 306 K [56].

The relative permittivity of the soil-water system can be estimated through use of a four-component mixture model of soil solids, air, free water, and bound water [28]. Fig. 7 shows the complex relative permittivities and emissivities of the soil-water system for the water transport case. Estimates of both relative permittivity and emissivity are based upon the temperature and moisture content of the first soil layer. The magnitudes of both real and imaginary parts of the complex relative permittivity exhibit a diurnal oscillation with a decreasing average [Fig. 7(a)] that correlates with soil moisture in the uppermost soil layer. These averages also decrease with increasing microwave frequency.

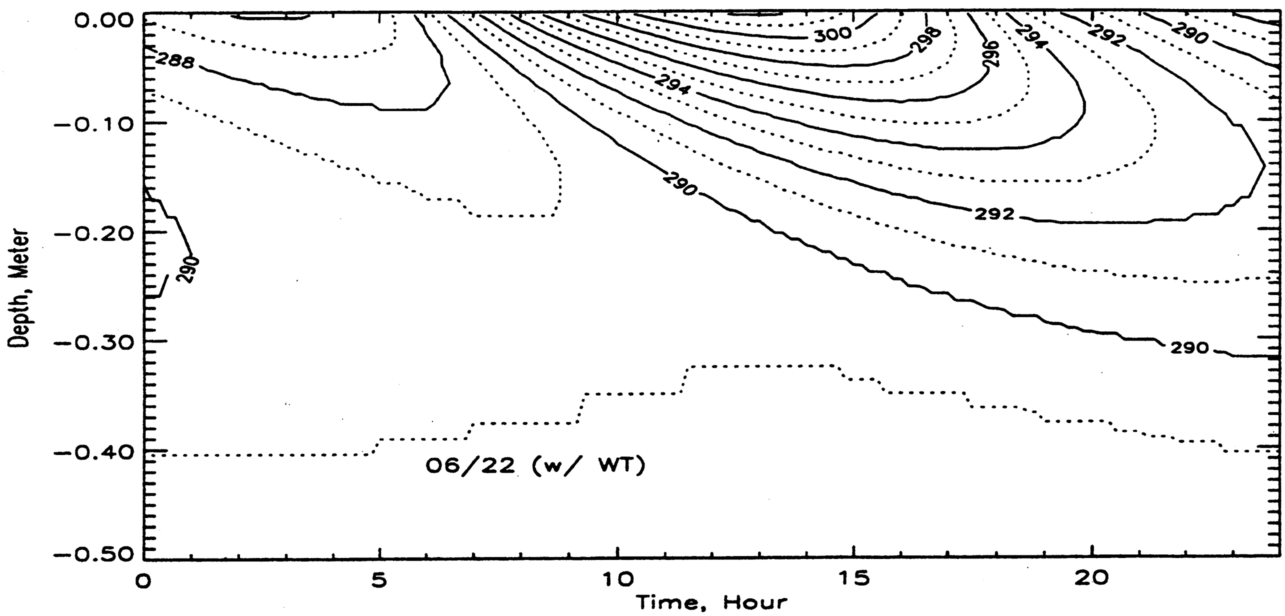

Fig. 6. Soil temperature profile on 06/22 for the water transport case.

The corresponding emissivities of soil based upon a quasispecular interface exhibit a diurnal oscillation with a slowly increasing average [Fig. 7(b)]. Their increase over the 60-day period for 19 and 37 GHz horizontal polarization is about 0.1, but is less for vertical polarization and for both polarizations at 85 GHz. An incidence angle of 53°, the incidence angle of the SSM/I radiometers, is used to compute the emissivity.

B. Soil Radiobrightnesses

The radiobrightness of bare, wet soil is

$$T_b(t) = e \cdot T_{\text{eff}}(t) \tag{40}$$

where e is the emissivity of the soil. The effective emitting temperature of the ground is

$$T_{\text{eff}}(t) = \kappa_e \sec\theta_t \int_0^{-\infty} e^{\kappa_e \sec\theta_t z} T_g(z,t)\, dz \tag{41}$$

where

κ_e extinction of the soil;
θ_t transmission angle;
$T_g(z,t)$ temperature of the soil at depth z.

The first order approximation to $T_{\text{eff}}(t)$ is

$$T_{\text{eff}}(t) = T_g(0,t) + \frac{1}{\kappa_e \sec\theta_t} \cdot \left(\frac{\partial T_g(z,t)}{\partial z}\right)_{z=0}. \tag{42}$$

As shown in [28], the diurnal extremes of the first-order terms over an annual cycle are on the order of ±0.3 K at 19 GHz for 17% moist soil and decrease with increasing frequency and water content.

Fig. 8(a) shows 60-day radiobrightness signatures for the water transport case with 19 GHz horizontal polarization. The 37 and 85 GHz results are not shown because they are similar to, but smaller in amplitude than, the 19 GHz results. The characteristics of vertically polarized brightnesses would be similar. The signatures are nearly linear with temperature except for a small, second-order effect caused by emissivity's dependence upon temperature. The change in diurnal average over the 60-day period is about 40 K for 19-GHz horizontal polarization, about 34 K for 37-GHz horizontal polarization, and about 26 K for 85-GHz horizontal polarization.

TABLE I
CHANGE IN THE DIURNAL AVERAGE RADIOBRIGHTNESS OVER THE 60-DAY SIMULATION FOR BOTH WATER TRANSPORT AND NO WATER TRANSPORT CASES AT 19, 37, AND 85 GHz HORIZONTAL POLARIZATION

Changes (K)	19 GHz	37 GHz	85 GHz
60-day w/ WT	39.8	33.9	25.9
60-day w/o WT	2.3	2.5	2.1

TABLE II
DIURNAL VARIATIONS IN RADIOBRIGHTNESS BETWEEN 2 P.M. AND 2 A.M. FOR BOTH WATER TRANSPORT AND NO WATER TRANSPORT CASES AT 19, 37, AND 85 GHz HORIZONTAL POLARIZATION

Variations (K)	19 GHz	37 GHz	85 GHz
1-day w/ WT	12.7	8.8	8.8
1-day w/o WT	2.3	-1.6	-1.6

Table I shows the maximum change in diurnal average radiobrightness over the 60-day simulation for both water transport and no water transport cases at 19, 37, and 85 GHz horizontal polarization. Radiobrightness at a fixed time in the diurnal cycle increases with day number because of a decrease in soil moisture. Similarly, daytime increases in maximum radiobrightness are also a response to decreases in liquid water content.

The largest variations in radiobrightness between 2 p.m. and the following 2 a.m. within the 60-day simulation are shown in Table II for both water transport and no water transport cases at 19, 37, and 85 GHz horizontal polarization.

The 60-day radiobrightness signatures for 19 GHz horizontal polarization for the no water transport case are shown in Fig. 8(b). The change in diurnal average radiobrightness

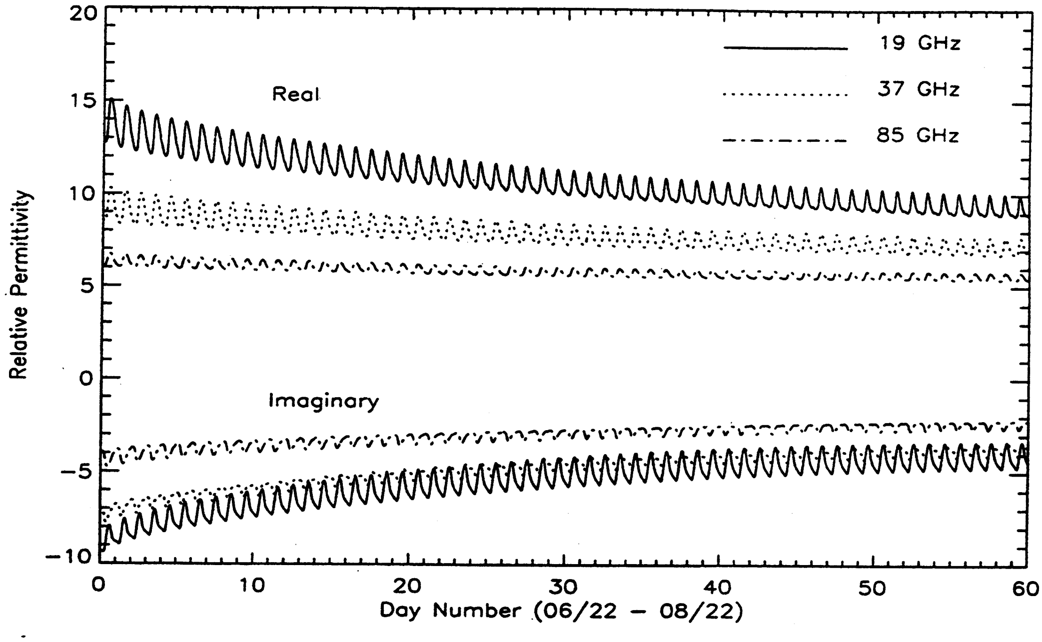

(a)

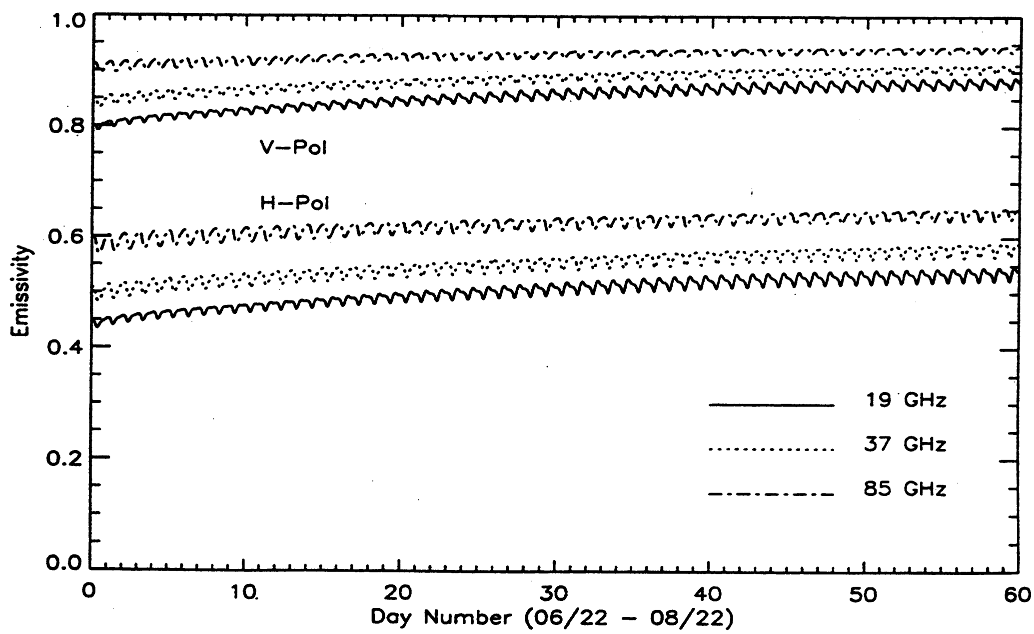

(b)

Fig. 7. (a) Complex relative permittivities of soil at the surface conditions of the water transport case.(b) Emissivities associated with (a).

over the 60-day period is within 3 K—much smaller than for the water transport case. The day-to-night variations in 19-GHz horizontal radiobrightness are weakly positive over the simulation period, while the equivalent variations for both 37 and 85 GHz are weakly negative. The contrast is caused by differing soil dielectric behavior with temperature at the three frequencies.

C. RTI Measure of Soil Moisture

Soil moisture is tied to radiometric signatures through its dominant influence upon diurnal soil temperatures and upon the dielectric properties of soil. Idso *et al.* [57] addressed the importance of soil moisture in determining the visible reflectance of bare soil. Heilman and Moore [58], [59] conducted a thermal infrared experiment to discriminate among various rock and soil types based upon the differences in the near-surface storage of moisture.

England *et al.* [25] proposed a radiobrightness thermal inertia (RTI) scheme for estimates of soil moisture, and concluded that of the SSM/I radiometer frequencies and polarizations, the 37.0 and 85.5 GHz, H-Polarized channels appear to be best suited to RTI. The RTI scheme was based on a

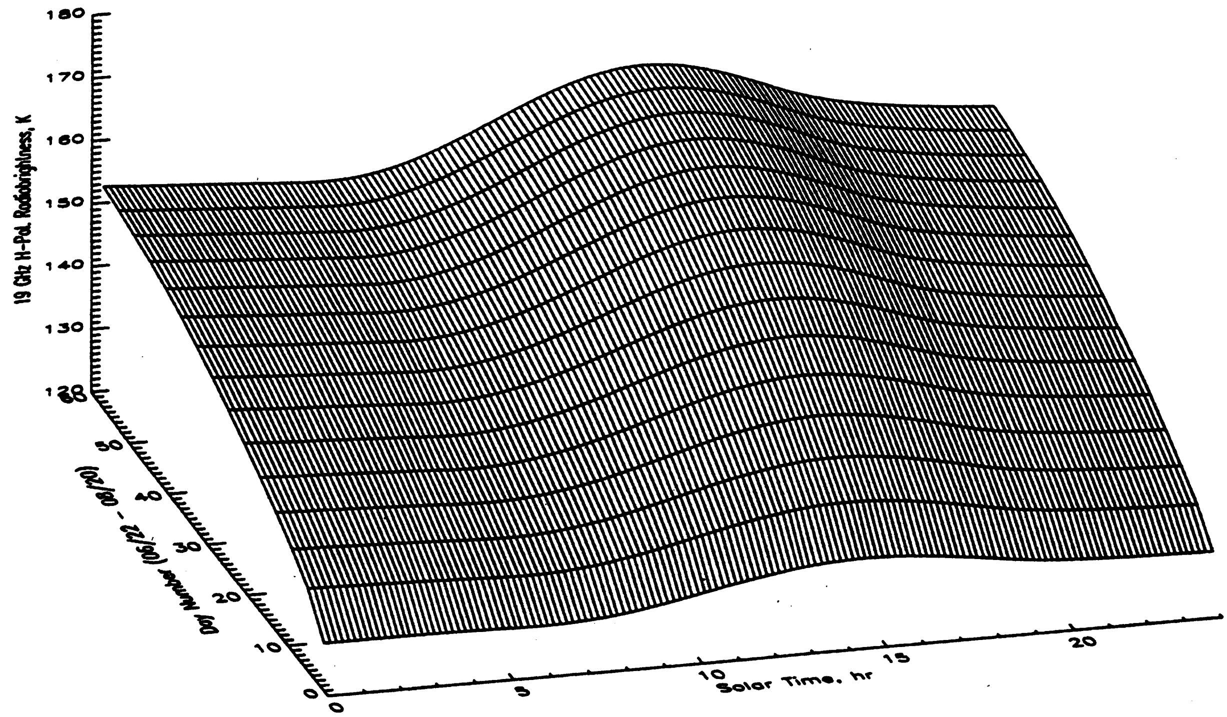

(a)

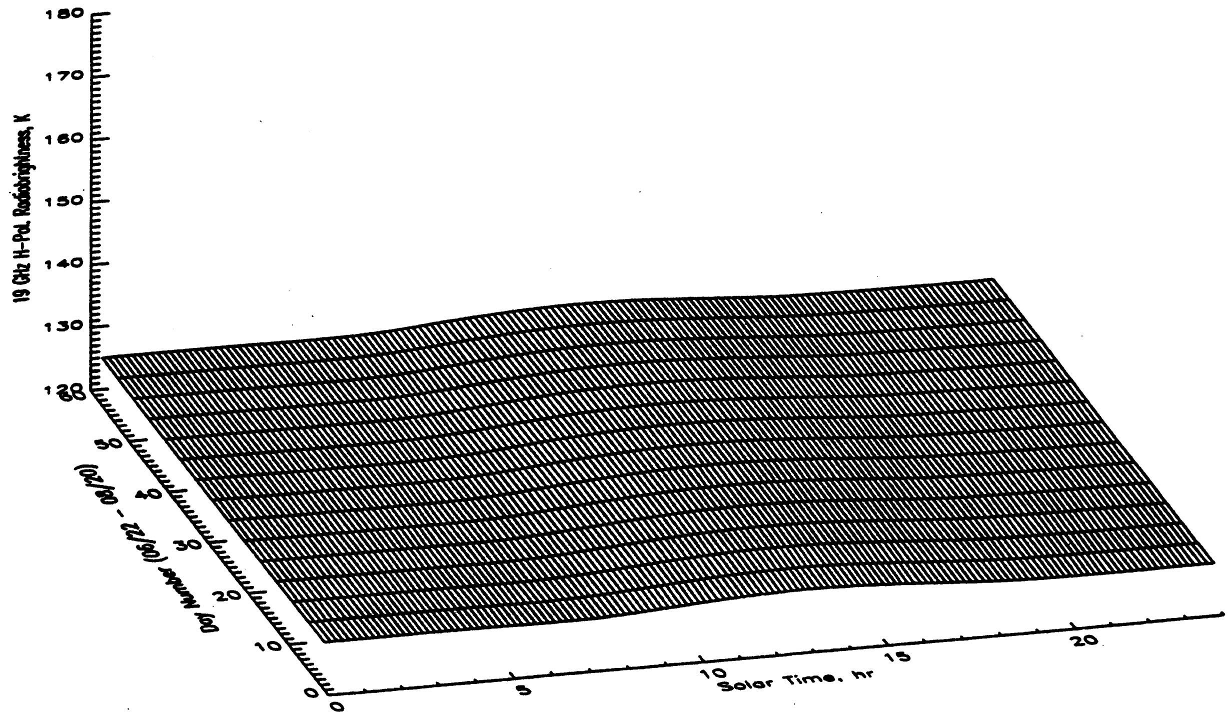

(b)

Fig. 8. Radiobrightness signatures for 19 GHz horizontal polarization (a) for the water transport case, and (b) for the no water transport case.

knowledge of the relationship between the change in day-night radiobrightness and the soil moisture content derived from the predictions of the Michigan Cold Region Radiobrightness (MCRR/diurnal) model of England [24]. The major features of the scheme were 1) soils with higher water content have a smaller change in day-night radiobrightness because of increased thermal inertia and decreased emissivity; 2) potential masking contributions to radiobrightness from sparse vegetation vary minimally in a diurnal cycle and so their contribution does not greatly change the day-night difference; and 3) sun-synchronous satellites overfly a region at nearly 12 hour intervals. Unlike the 1-DH model, the MCRR/diurnal model

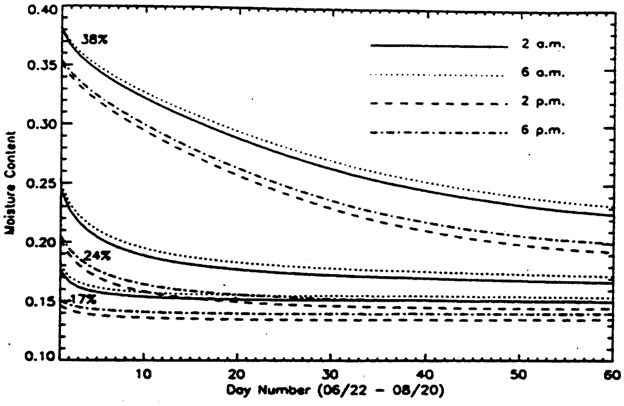

(a)

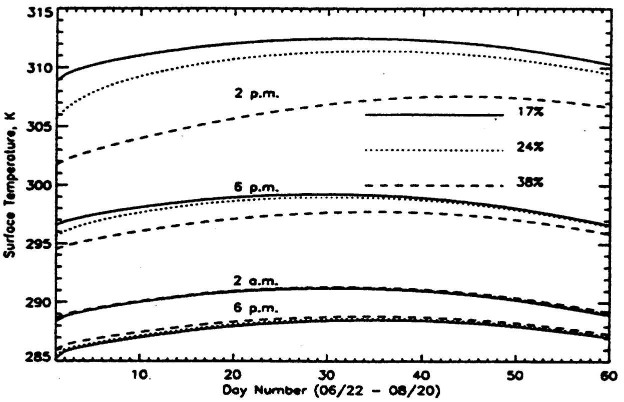

(b)

Fig. 9. (a) Soil moisture content at the surface at four times: 2 a.m., 6 a.m., 2 p.m., and 6 p.m. for the 38%, 24%, and 17% cases (all with water movement in the soil). (b) Surface temperature at four times: 2 a.m., 6 a.m., 2 p.m., and 6 p.m. for the 38%, 24%, and 17% cases.

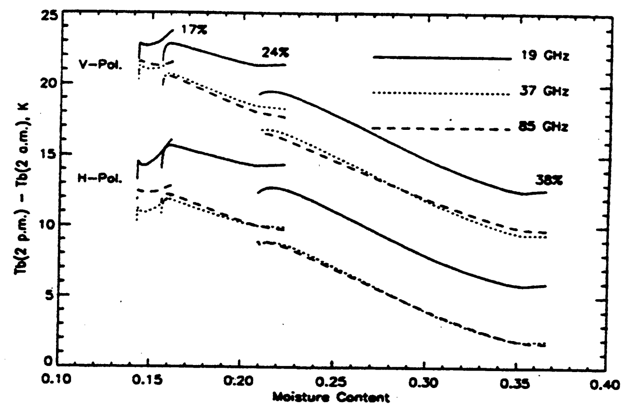

(a)

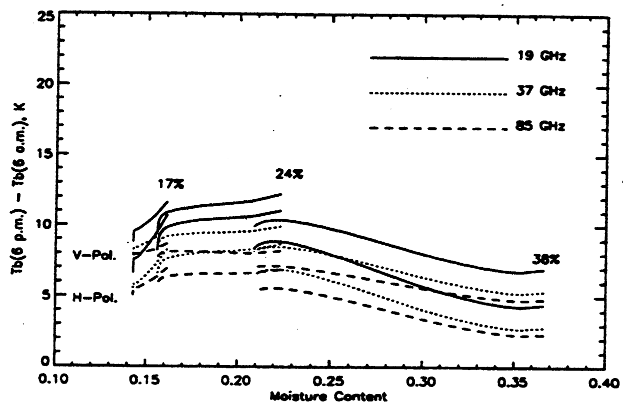

(b)

Fig. 10. (a) Radiobrightness differences between 2 p.m. and 2 a.m. for the 38%, 24%, and 17% cases. (b) Radiobrightness differences between 6 p.m. and 6 a.m. for the 38%, 24%, and 17% cases.

ignored the dependences of thermal and moisture profiles upon latent heat transfer, historical weather forcing at the land-air interface, and soil water movements.

To reexamine the feasibility of the RTI measure of soil moisture over a wide range of moisture contents, we ran the 1-DH model for the cases with drier initial moisture contents of 24% and 17% for the same 60-day period as we did for the 38% case. Fig. 9 shows the surface soil moisture contents and temperatures at 2 a.m., 6 a.m., 2 p.m., and 6 p.m. for the 38%, 24%, and 17% cases (all with vertical water movement in soil). We see that (1) soil moisture contents decrease monotonically with day number for the three dry-down simulations; (2) soil moisture decreases rapidly in the beginning few days of the 60-day period, but slowly in the rest of the same period; and (3) soil moisture contents never go below 13% because evaporation ceases at the wilting point of 13%. Fig. 9(b) shows that the surface temperatures increase with time for about the first 40 days and decrease with time for the rest of the simulation period. The temperature differences between 2 p.m. and 2 a.m. are largest for the driest soil—about 21 K over the 60-day period for the 17% case, about 20 K for the 24% case, and about 17 K for the 38% case.

Fig. 10 concerns the radiobrightness differences between 2 p.m. and 2 a.m., and between 6 p.m. and 6 a.m. for 19, 37, and 85 GHz horizontal and vertical polarization. The 60-day dry-down brightness differences are shown for the 38%, 24%, and 17% initial moisture contents. The horizontal axis represents the averages of soil moisture contents between 2 p.m. and 2 a.m., and between 6 p.m. and 6 a.m.. Note that the radiobrightness differences generally increase with decreased moisture content for the dry-down simulations in the 38% and 24% cases. Each of these differences decrease at the end of their simulation period where the decrease in soil moisture with time is small and diurnal temperature extremes are diminished as fall approaches. Only the final decrease is evident in the 17% case where there is little free water available. If we connect the three ending points of the dry-down curve, and the three starting points of the same curve, respectively, there would be the six strips in Fig. 10(a). Each strip represents the area that radiobrightness differences may appear during a dry-down process. The slope of the strips is an estimate of the sensitivity of the RTI method to soil moisture, while the width of the strips in the vertical direction is an indicator of uncertainty caused by time since the last infiltration. Fig. 10(a) demonstrates that the three frequencies have about the same sensitivities to soil moisture in those ideal cases of quasispecular interfaces. Fig. 10(a) and (b) show that the RTI scheme correlates with soil moisture for the 2 p.m.–2 a.m. case, but is insensitive to soil moisture for the 6 p.m.–6 a.m. case.

The magnitudes of RTI from the current model are smaller than those from the England *et al.* [25] by approximately 6 K for horizontal polarization, and by about 20 K for vertical polarization. Such significant discrepancies between the two models demonstrate the importance of including latent heat transfer and historic weather forcing at the land-air interface, and of coupling water movement with temperature gradients in the thermal model. This diminished sensitivity casts the utility of the RTI method in some doubt and, because RTI is more sensitive than a thermal infrared-based measure of thermal inertia, it also explains the difficulty of deriving soil moisture from a TIR-based model.

IV. Conclusion

We have presented a 1-DH/R model for bare, unfrozen, moist soils. The 1-DH model includes coupled thermal and moisture transport within the soil and at the land-air interface, and soil thermal properties are treated realistically as functions of temperature and moisture. The radiobrightness model is based upon the temperature and moisture content of a quasi-specular upper soil layer. The physical fidelity of the 1-DH/R model affords some confidence in its predictions. Certainly, the 1-DH/R model is superior to our earlier model, the MCRR model, which successfully guided our earlier investigations of the radiobrightness of freezing and thawing soils.

The most significant prediction of the 60-day dry-down simulation is that SSM/I radiobrightnesses are sensitive to the dry-down process. The change for the 19 GHz horizontal polarization case was nearly 40 K over the 60-day period. This large dynamic range suggests that radiobrightness observations can be used to improve a model state estimate—at least for this simple case—if the precipitation history is known.

While RTI is sensitive to soil moisture, the sensitivity may not be significant enough for the practical use in field inversions of soil moisture for bare or sparsely-vegetated lands. As vegetation cover increases, the interpretation of radiobrightness will become more complex. Vegetation that exceeds ~ 2 kg/m^2 column density appears nearly black at the SSM/I frequencies [60] so that enhancements in emissivity with water content are lost. Furthermore, vegetation actively maintains wetness levels by reducing transpiration as soils dry. Reduced transpiration will result in greater day-night differences in canopy temperature and radiobrightness, but the signature is sufficiently unique that its interpretation in terms of soil moisture may be difficult. Lower, more penetrating frequencies, like L-band, would greatly ease the interpretation where there is significant vegetation.

We recognize the need to validate the 1-DH/R model experimentally. Our group will conduct a field experiment on the prairie grassland near Sioux Falls, SD, during the summer of 1996. Field data will be taken on both grassland and artificially bare soil at half-hour intervals throughout the growing season. Measurements will include horizontally and vertically polarized radiobrightnesses at SSM/I frequencies (only one polarization for 85 GHz), soil temperatures, soil and canopy moisture, soil heat flux, 10 m wind speed and direction, air temperature, relative humidity, downwelling and upwelling shortwave radiation, downwelling longwave radiation, precipitation, thermal infrared canopy temperature, and Bowen ratio.

References

[1] P. R. Rowntree and J. R. Bolton, "Simulation of the atmospheric response to soil moisture anomalies over Europe," *Q. J. R. Meteorol. Soc.*, vol. 109, pp. 501–526, 1983.

[2] W. M. Cunnington and P. R. Rowntree, "Simulation of the Saharan atmosphere-dependence on moisture and albedo," *Q. J. R. Meteorol. Soc.*, vol. 112, pp. 971–999, 1986.

[3] J.-F. Mahfouf, E. Richard, and P. Mascart, "The influence of soil and vegetation on the development of mesoscale circulations," *J. Appl. Meteor.*, vol. 26, pp. 1483–1495, 1987.

[4] D. P. Rowell and C. Blondin, "The influence of soil wetness distribution on short-range rainfall forecasting in the West African Sahel," *Q. J. R. Meteorol. Soc.*, vol. 116, pp. 1471–1485, 1990.

[5] Y. Mintz and G. K. Walker, "Global fields of soil moisture and land surface evapotranspiration derived from observed precipitation and surface air temperature," *J. Appl. Meteor.*, vol. 32, pp. 1305–1334, Aug. 1993.

[6] C. B. Smith, M. N., Lakhtakia, W. J. Capehart, and T. N. Carlson, "Initialization of soil-water content in regional-scale atmospheric prediction models," *Bull. Amer. Meteor. Soc.*, vol. 75, pp. 585–593, 1994.

[7] X. Liang, D. P. Lettenmaier, E. F. Wood, and S. J. Burges, "A simple hydrologically based model of land surface water and energy fluxes for general circulation models," *J. Geophys. Res.*, vol. 99, pp. 14 415–14 428, 1994.

[8] R. E. Dickinson, A. Henderson-Sellers, P. J. Kennedy, and W. F. Wilson, "Biosphere-atmosphere transfer scheme (BATS) for the NCAR community climate model," *Tech. Note NCAR/TN-275 + STR*, Nat. Center Atmos. Res., Boulder, CO, 1986.

[9] P. J. Sellers, Y. Mintz, Y. C. Sud, and A. Dalcher, "A simple biosphere model (SiB) for use within general circulation models," *J. Atmos. Sci.*, vol. 43, pp. 505–531, Mar. 1986.

[10] J.-F. Mahfouf, "Analysis of soil moisture from near-surface parameters: A feasibility study," *J. Appl. Meteor.*, vol. 30, pp. 1534–1547, 1991.

[11] F. Bouttier, J.-F. Mahfouf, and J. Noilhan, "Sequential assimilation of soil moisture from atmospheric low-level parameters, Part I: Sensitivity and calibration studies," *J. Appl. Meteor.*, vol. 32, pp. 1335–1351, Aug. 1993.

[12] ——, "Sequential assimilation of soil moisture from atmospheric low-level parameters, Part II: Implementation in a mesoscale model," *J. Appl. Meteor.*, vol. 32, pp. 1352–1364, Aug. 1993.

[13] J. R. Wang and T. J. Schmugge, "An empirical model for the complex dielectric permittivity of soils as a function of water content," *IEEE Trans. Geosci. Remote Sensing*, vol. GE-18, pp. 288–295, Oct. 1980.

[14] M. C. Dobson, F. T. Ulaby, M. T. Hallikainen, and M. A. El-Rayes, "Microwave dielectric behavior of wet soil—Part II: Dielectric mixing models," *IEEE Trans. Geosci. Remote Sensing*, vol. GE-23, pp. 35–46, Jan. 1985.

[15] M. Hallikainen, F. T. Ulaby, M. C. Dobson, M. El-Rayes, and L.-K. Wu, "Microwave dielectric behavior of wet soil—Part I: Empirical models and experimental observations," *IEEE Trans. Geosci. Remote Sensing*, vol. GE-23, pp. 25–34, Jan. 1985.

[16] T. J. Schmugge, P. E. O'Neill, and J. R. Wang, "Passive microwave soil moisture research," *IEEE Trans. Geosci. Remote Sensing*, vol. GE-24, pp. 12–22, Jan. 1986.

[17] T. J. Jackson and R. E. O'Neill, "Attenuation of soil microwave emission by corn and soybeans at 1.4 and 5 GHz," *IEEE Trans. Geosci. Remote Sensing*, vol. 28, pp. 978–980, 1990.

[18] J. F. Galantowicz and A. W. England, "Radiobrightness signatures of energy balance processes: Melt/freeze cycles in snow and prairie grass covered ground," in *Proc. IGARSS'95 Symp.*, Florence, Italy.

[19] J. Hollinger, R. Lo, G. Poe, R. Savage, and J. Pierce, *Special Sensor Microwave/Imager User's Guide*, Naval Res. Lab., Washington, DC, 1987.

[20] K. Watson, "Geologic applications of thermal infrared images," *Proc. IEEE*, vol. 63, pp. 370–379, 1975.

[21] A. B. Kahle, "A simple thermal model of the earth's surface for geologic mapping by remote sensing," *J. Geophys. Res.*, pp. 380–387, vol. 11, Apr. 10, 1977.

[22] J. C. Price, "Thermal inertia mapping: A new view of the Earth," *J. Geophys. Res.*, vol. 82, pp. 2582–2590, 1977.

[23] ——, "The potential of remotely sensed thermal infrared data to infer surface moisture and evaporation," *Water Resources Res.*, vol. 16, pp. 787–795, 1980.

[24] A. W. England, "Radiobrightness of diurnally heated, freezing soil," *IEEE Trans. Geosci. Remote Sensing*, vol. 28, pp. 464–476, July 1990.
[25] A. W. England, J. F. Galantowicz, and M. S. Schretter, "The radiobrightness thermal inertia measure of soil moisture," *IEEE Trans. Geosci. Remote Sensing*, vol. 30, pp. 132–139, Jan. 1992.
[26] A. W. England, J. F. Galantowicz, and B. W. Zuerndorfer, "A volume scattering explanation for the negative spectral gradient of frozen soil," in *Proc. IGARSS'91 Symp.*, Espoo, Finland, pp. 1175–1177.
[27] Y.-A. Liou and A. W. England, "An annual model of SSM/I radiobrightness for dry soil," in *Proc. IGARSS'92 Symp.*, Houston, TX.
[28] ——, "Annual temperature and radiobrightness signatures for bare soils," *IEEE Trans. Geosci. Remote Sensing*, vol. 34, pp. 981–990, July 1996.
[29] J. R. Philip and D. A. de Vries, "Moisture movement in porous materials under temperature gradients," *Trans. Amer. Geophys. Union*, vol. 38, pp. 222–232, Apr. 1957.
[30] D. A. de Vries, "Simultaneous transfer of heat and moisture in porous media," *Trans. Amer. Geophys. Union*, vol. 39, pp. 909–916, Oct. 1958.
[31] G. W. Gee, "Water movement in soils as influenced by temperature gradients," Ph.D. dissertation, Washington State Univ., Pullman, WA, 1966, Diss. Abstr. 66-13560.
[32] D. K. Cassel, D. R. Nielsen, and J. W. Biggar, "Soil-water movement in response to imposed temperature gradients," *Soil Sci. Soc. Amer. Proc.*, vol. 33, pp. 493–500, 1969.
[33] R. D. Jackson, R. J. Reginato, B. A. Kimball, and F. S. Nakayama, "Diurnal soil-water evaporation: comparison of measured and calculated soil water fluxes," *Soil Sci. Soc. Amer. Proc.*, vol. 38, pp. 861–866, 1974.
[34] B. A. Kimball, R. D. Jackson, R. J. Reginato, F. S. Nakayama, and S. B. Idso, "Comparison of field-measured and calculated soil-heat fluxes," *Soil Sci. Soc. Amer. Proc.*, vol. 40, pp. 18–25, 1976.
[35] P. C. D. Milly and P. S. Eagleson, "The coupled transport of water and heat in a vertical soil column under atmospheric excitation," Tech. Rep. 258, R. M. Parsons Lab., Dept. Civil Eng., Mass. Inst. Technol., Cambridge, MA, 1980.
[36] P. C. D. Milly and P. S. Eagleson, "Parameterization of moisture and heat fluxes across the land surface for use in atmospheric general circulation models," Tech. Rep. 279, R. M. Parsons Lab., Dept. Civil Eng.g, Mass. Inst. Technol., Cambridge, MA, 1982.
[37] P. C. D. Milly, "Moisture and heat transport in hysteretic, inhomogeneous porous media: A matric head based formulation and a numerical model," *Water Resources Res.*, vol. 18, pp. 489–498, June 1982.
[38] ——, "A simulation analysis of thermal effects on evaporation from soil," *Water Resources Res.*, vol. 20, pp. 1087–1098, Aug. 1984.
[39] L. B. Bach, "Soil water movement in response to temperature gradients: Experimental measurements and model evaluation," *Soil Sci. Soc. Amer Proc.*, vol. 56, pp. 37–46, 1992.
[40] O. N. Abdel-Hadi and J. K. Mitchell, "Coupled heat and water flows around buried cables," *J. Geotech. Eng. Div.*, vol. 107, pp. 1461–1487, 1981.
[41] D. J. Shah, J. W. Ramsey, and M. Wang, "An experimental determination of the heat and mass transfer coefficients in moist, unsaturated soils," *Int. J. Heat Mass Transf.*, vol. 27, pp. 1075–1085, 1984.
[42] H. R. Thomas, "Nonlinear analysis of heat and moisture transfer in unsaturated soil," *J. Eng. Mech.*, vol. 113, pp. 1163–1180, 1987.
[43] J. Ewen and H. R. Thomas, "Heating unsaturated medium sand," *Geotechnique*, vol. 39, pp. 455–470, 1989.
[44] H. R. Thomas and S. D. King, "Coupled heat and mass heat transfer in unsaturated soil—A potential-based solution," *Int. J. Numer. Anal. Meth. Geomech.*, vol. 16, pp. 757–773, 1992.
[45] D. A. de Vries, "Thermal properties of soils," in *Physics of Plant Environment*, W. R. van Wijk, Ed. Amsterdam, The Netherlands, North-Holland, pp. 210–235, 1963.
[46] S. Lai, J. M. Tiedje, and A. E. Erickson, "In situ measurement of gas diffusion coefficients in soils," *Soil Sci. Soc. Amer. Proc.*, vol. 40, pp. 3–6, 1976.
[47] C. Rossi and J. R. Nimmo, "Modeling of soil water retention from saturation to oven dryness," *Water Resources Res.*, vol. 30, pp. 701–708, Mar. 1994.
[48] P. J. Camillo, R. J. Gurney, and T. J. Schmugge, "A soil and atmospheric boundary layer model for evapotranspiration and soil moisture studies," *Water Resources Res.*, vol. 19, pp. 371–380, 1983.
[49] W. H. Press, B. P. Flannery, S. A. Teukolsky, W. T. Vetterling, *Numerical Recipes (FORTRAN)*. Cambridge, U.K.: Cambridge Univ. Press, 1989, p. 702.
[50] Y. Mualem, "A new model for predicting the hydraulic conductivity of unsaturated porous media," *Water Resources Res.*, vol. 12, pp. 513–522, June 1976.
[51] M. T. van Genuchten, "A closed-form equation for predicting the hydraulic conductivity of unsaturated flow," *Soil Sci. Soc. Amer. Proc.*, vol. 44, pp. 892–898, 1980.
[52] J. R. Nimmo, Comment "A consistent set of parametric models for the two-phase flow of immiscible fluids in the subsurface," *Water Resources Res.*, vol. 27, pp. 661–662, 1991.
[53] P. J. Ross, J. Williams, and K. L. Bristow, "Equation for extending water-retention curves to dryness," *Soil Sci. Soc. Amer. Proc.*, vol. 55, pp. 923–927, 1991.
[54] R. H. Brooks and A. T. Corey, "Properties of porous media affecting fluid flow," *J. Irrig. Drain. Div. Amer. Soc. Civ. Eng.*, vol. 92, pp. 61–87, 1966.
[55] I. N. Nassar and R. Horton, "Water transport in unsaturated nonisothermal salty soil: II. Theoretical development," *Soil Sci. Soc. Am. Proc.*, vol. 53, pp. 1330–1337, 1989.
[56] F. T. Ulaby, R. K. Moore, and A. K. Fung, *Microwave Remote Sensing, Active and Passive*. Norwood, MA: Artech House, 1986, vol. III.
[57] S. B. Idso, R. D. Jackson, R. J. Reginato, B. A. Kimball, and F. S. Nakayama, "The dependence of bare soil on soil water content," *J. Appl. Meteror.*, vol. 14, pp. 109–113, 1975.
[58] J. L. Heilman and D. G. Moore, "HCMM detection of high soil moisture areas," *Remote Sens. Environ.*, vol. 11, pp. 73–76, 1981.
[59] ——, "Evaluating near-surface soil moisture using heat capacity mapping mission data," *Remote Sens. Environ.*, vol. 12, pp. 117–121, 1982.
[60] A. W. England and J. F. Galantowicz, "Observed and modeled radiobrightness of prairie grass in early fall," in *Proc. IGARSS'95 Symp.*, Florence, Italy.

Yuei-An Liou (S'91–M'96) received the B.S. degree in electrical engineering from National Sun Yat-Sen University, Kaohsiung, Taiwan, R.O.C., the M.S.E. degree in electrical engineering, the M.S. degree in atmospheric and space sciences, and the Ph.D. degree in electrical engineering and atmospheric and space sciences from The University of Michigan, Ann Arbor, in 1987, 1992, 1994, and 1996, respectively.

He is currently an Associate Professor at the Center for Space and Remote Sensing Research, National Central University, Chung-Li, Taiwan. From 1989 to 1990, he was a research assistant with the National Taiwan University Robotics Laboratory, Taipei. From 1991 to 1996, he was a Graduate Research Aassistant at the University of Michigan Radiation Laboratory working in the field of geophysical remote sensing. Since August 1996, he has been with the National Central University. His interests include energy and moisture transport in subsurface porous media, land-atmosphere interactions, microwave radiometric studies of terrains, ocean, and atmosphere, and the coupling of these interactions to atmospheric models.

Anthony W. England (M'87–SM'89–F'95) received the B.S. and M.S. degrees in earth sciences from the Massachusetts Institute of Technology (MIT), Cambridge, in 1965 and the Ph.D. degree in geophysics from MIT in 1970.

He is Professor of Electrical Engineering and Computer Science, Professor of Atmospheric, Oceanic and Space Science, and Associate Dean of the Rackham School of Graduate Studies at the University of Michigan, Ann Arbor. He teaches electromagnetics and remote sensing geophysics. His research has spanned scattering theory as applied to radio emitters, the development and application of ice-sounding radar for the study of glaciers in Alaska and during two field seasons in Antarctica, and, currently, the assimilation of satellite microwave data in land-surface process models. He was a scientist/astronaut during two periods with NASA, where he served on the support crews of Apollo 13 and Apollo 16, flew as a Mission Specialist on Spacelab 2 in 1985, and was Program Scientist for the Space Station during 1986 and 1987. He was a Research Geophysicist and Deputy Chief of the Office of Geochemistry and Geophysics during seven years with the U.S. Geological Survey, and was a Visiting Adjunct Professor at Rice University, Houston, TX, before joining the University of Michigan in 1988. He has been as Associate Editor for the *Journal of Geophysical Research*.

Dr. England is a member of the American Geophysical Union. He is a member of the National Research Council's Space Studies Board, and has served on several federal committees concerned with Antarctic policy, nuclear waste containment, and federal science and technology.